On the quiet-time occurrence rates, severity and origin of L-band ionospheric scintillations observed from low-to-mid latitude sites located in Puerto Rico

J. Gomez Socola¹, J. Sousasantos¹, F. S. Rodrigues¹, C.G.M. Brum², P. Terra², A. O. Moraes³, and R. Eastes⁴

- 1. W. B. Hanson Center for Space Sciences, The University of Texas at Dallas, Richardson, TX. USA
- 2. Arecibo Observatory, Puerto Rico
- 3. Instituto de Aeronáutica e Espaço (IAE), São José dos Campos, SP, Brazil
- 4. Laboratory for Atmospheric and Space Physics, University of Colorado Boulder, Boulder, CO, USA

Key points:

- GNSS-based monitors were deployed in Puerto Rico PR (~24.5° N dip latitude) and detected L-band scintillation on ~80% of geomagnetically quiet nights.
- Cases of very intense amplitude scintillation ($S_4 \sim 1.0$) were commonly observed and were accompanied by large TEC depletions.
- The latitudinal extent of EPBs and of the northern crest of the EIA create conditions for the strong quiet-time scintillations observed by GNSS receivers in PR.

Abstract: In December 2021 three Global Navigation Satellite System (GNSS) ionospheric scintillation and total electron content (TEC) monitors were installed in Puerto Rico (~24.5° N dip latitude). The installation is part of an effort to better understand the occurrence of ionospheric irregularities and scintillation at mid-latitudes. Puerto Rico (PR) is commonly referred to as being located at mid-latitudes or at the boundary between low and mid-latitudes. Previous reports already presented observations of ionospheric irregularities and scintillation detected from PR. These observations, however, were limited in number. Additionally, the reports related the observed scintillation and irregularities events with different types of midlatitude ionospheric disturbances. Here we present results from the analyses of the first three months of observations, December 21st, 2021 to March 20th, 2022. The analyses focus on the occurrence rate, severity and origin of scintillation detected on the signals tracked by the PR monitors during geomagnetically quiet times. We show that, out of the 43 geomagnetically quiet nights, 34 (~80%) showed the occurrence of L-band scintillation. The results also indicate the recurrent existence of severe scintillation ($S_4 \sim 1.0$) accompanied by large TEC depletions. The temporal evolution of the observed scintillation showed that scintillation-causing plasma irregularities first occurred near the magnetic equator and propagated towards PR (reaching up to $\sim 22^{\circ}$ dip latitude). Simultaneous space-based observations of the ionospheric F-region peak electron densities made by the GOLD mission confirmed that the guiet-time scintillation observed by the monitors in PR was associated with equatorial plasma bubbles. GOLD observations also show enhanced background F-region densities at the location of the ionospheric pierce points (IPPs) of the affected GNSS signals, indicating conditions that favor the occurrence of intense scintillation.

Keywords: Ionosphere, GNSS, scintillation, low latitudes, mid-latitudes, equatorial plasma bubbles.

1. Introduction

Ionospheric irregularities and their effects on radio signals crossing the upper atmosphere have been reported for decades (e.g., Yeh and Swenson Jr., 1959). However, since the announcement of the full operational capability of the Global Positioning System (GPS) and the subsequent widespread use of satellite-based systems for positioning and other technological purposes, the interest in these phenomena has increased substantially (Beach and Kintner, 2001). One of the most important effects of ionospheric irregularities on transionospheric radio signals is the so-called ionospheric scintillation (Briggs, 1964; Yeh and Liu, 1982). Ionospheric scintillation can be described as amplitude and/or phase fluctuations produced by variations in the ionospheric plasma density occurring along the signal path (Yeh and Liu, 1982; Beach and Kintner, 2001). Ionospheric irregularities and scintillation are significant components of space weather.

The phenomenon of scintillation is often said to occur more frequently at low and high geomagnetic latitudes (Aarons, 1982; Basu et al., 1988). At high latitudes many phenomena are believed to generate scintillation on the signals (Beach and Kintner, 2001) including polar cap patches. At low latitudes, scintillation is associated predominantly with equatorial spread F (ESF). ESF is the term used when referring to a wide range of ionospheric irregularities produced by the generalized Rayleigh-Taylor (GRT) instability (Sultan, 1996). It is well-known that large scale (10-100s of km) ionospheric plasma depletions known as equatorial plasma bubbles (EPBs) develop in the bottomside F-region at the magnetic equator due to the GRT instability. The EPBs rise vertically extending along magnetic field lines to low latitudes. Secondary plasma instabilities produce smaller scale irregularities that accompany the EPBs (Hysell, 2000). The scintillation events caused by EPBs are known to be the most intense in the Earth's ionosphere (Aarons, 1982; Jiao and Morton, 2015; Juan et al., 2018).

Because scintillation occurs more frequently at low and high latitudes, significantly less instrumentation and efforts have been dedicated to mid-latitude studies. Nevertheless, the occurrence of ionospheric irregularities at mid-latitudes has been reported (e.g., Perkins, 1973; Fukao et al., 1991; Kelley and Fukao, 1991; Mathews et al., 2001a, 2001b; Martinis and Mendillo, 2007; Martinis et al., 2009). Furthermore, some studies revealed the occurrence of mid-latitude scintillation with severities that were comparable to those at low latitudes (e.g., Karasawa et al., 1985; Basu et al., 2001; Ledvina et al., 2002). In some cases, the observed mid-latitude scintillation events were associated with auroral activity and originating at high latitudes (e.g., Afraimovich et al., 2004, 2009; Jakowski et al., 2007). There are also reports of mid-latitude scintillation and its association with ESF and EPBs (Vadakke Veettil et al., 2017).

The source of irregularities producing scintillations events at low-to-mid latitudes does not always reach a consensus. For instance, Mendillo et al. (1997) reported a plasma depletion captured on the 3rd of May 1995, by an all-sky airglow imager in Arecibo, Puerto Rico and hypothesized that it was an EPB reaching altitudes around 2,500 km at the magnetic equator. This EPB could have caused strong scintillation at low-to-mid latitudes. Kelley et al. (2000b), presented airglow observations made from Arecibo on 22-23 November 1997, that also indicated the occurrence of plasma depletions. Based on features (local time occurrence and drift direction) they could not associate this event with EPBs. Both events, however, occurred during geomagnetically disturbed conditions.

More recently, Martinis et al. (2015) presented observations of depleted structures over geomagnetic latitudes of 40° using airglow all-sky data. They argued that this was an extreme

EPB reaching the mid-latitudes. Kil et al. (2016) analyzed the same event and commented that the source of the ionospheric irregularities was unlikely to be an extreme EPB, but a "super" Medium-Scale Travelling Ionospheric Disturbance (MSTID) instead. Rodrigues et al. (2021) showed that this event caused strong scintillation at mid-latitudes.

Since then, an increasing number of studies have reported plasma irregularities over midlatitudes (e.g., Cherniak and Zakharenkova, 2016, 2022; Katamzi-Joseph et al., 2017; Aa et al., 2018; Li et al., 2018; Zakharenkova and Cherniak, 2020, 2021; and Sori et al., 2022). All the events discussed in these studies occurred under geomagnetically disturbed conditions and most of these are case studies. A comprehensive investigation, evaluating the mid-latitude scintillation activity during geomagnetic quiet periods is still required.

Therefore, as part of an effort to understand the coupling between low and mid-latitudes with emphasis on the occurrence of ionospheric scintillation we deployed three ground-based monitors over Puerto Rico (~24.5° N dip latitude). In this work we report results of an analysis of a 3-month campaign carried out from December 21st, 2021, to March 20th, 2022, focusing on observations made during geomagnetically quiet days. The occurrence rates, the severity of the scintillation events, its spatiotemporal distribution, and the possible sources of the plasma irregularities causing the observed scintillation are discussed. In support of the ground-based observations, peak electron density data from the Global-scale Observations of the Limb and Disk (GOLD) were used to evaluate the sources of the irregularities leading to the scintillation in the Global Navigation Satellite System (GNSS) signals.

In summary, the effort presented here contributes to the state of knowledge by providing a new comprehensive set of ionospheric scintillation and total electron content (TEC) measurements made by monitors deployed in Puerto Rico. It also contributes, through analyses of these measurements, to a better understanding of the occurrence of intermediate scale (few 100s of meters) irregularities and to a better understanding about the severity of GNSS scintillation in a region that is boundary between low and mid latitudes. Additionally, in combination with GOLD observations, the effort contributes to a better understanding of the source of ionospheric density perturbations and scintillations observed from Puerto Rico.

2. Instrumentation and measurements

In order to determine the occurrence rate, severity, spatiotemporal distribution, and the possible sources of the scintillation observed in the region of Puerto Rico (PR), ground-based monitors were used in association with space-based imaging data. The ground-based observations were made by ScintPi 3.0 monitors. ScintPi 3.0 is a low-cost GNSS-based ionospheric scintillation and total electron content (TEC) monitor developed at UT Dallas (Gomez Socola and Rodrigues, 2022). In addition, auxiliary measurements provided by the GOLD mission (Eastes et al., 2017) were also presented in this investigation.

For this study we analyzed measurements made during an observation campaign between December 21^{st} , 2021, and March 20^{th} , 2022, the first three months of observations made by the system. This period coincides with the rising of the current solar cycle when the decametric solar flux index (F10.7) varied from ~81 up to 136 Solar Flux Units [1 SFU = 10^{-22} W/(m²Hz)].

Also, we were interested in measurements made during geomagnetically quiet conditions, therefore avoiding contributions from the disturbance dynamo and penetration electric fields, that could alter the ordinary ionospheric electrodynamics (e.g., Wolf, 1970; Blanc and

Richmond, 1980; Senior and Blanc, 1984). For that purpose, we restricted our analyses to measurements when the Kp did not exceed 3 during the nighttime period of interest (19:00 LT to 07:00 LT) as well as during the previous 24 hours. Local time (LT) in this report refers to Atlantic Standard Time (AST), with AST = UT - 4 hours.

2.1 ScintPi 3.0 measurements

Three ScintPi 3.0 monitors were deployed in Puerto Rico with the purpose of measuring ionospheric irregularities and scintillation activity in a region that has been referred to as being located at mid-latitudes or at the boundary between low and mid-latitudes (e.g., Kelley et al., 2000a, 2004; Urbina et al., 2000; Hysell et al., 2018). In addition to measuring scintillation, these distributed receivers will also allow future investigations related to spatial (local) variations in TEC.

The monitors have been distributed over Puerto Rico, in Arecibo – AO (66.75°W, 18.34°N, dip latitude: 24.65°N), Quebradillas – QB (66.91°W, 18.46°N, dip latitude: 24.81°N) and Culebra – CU (65.30°W, 18.33°N, dip latitude: 24.15°N) and started to make measurements in December 2021.

ScintPi 3.0 can track signals at two frequencies (L1 \sim 1.6 GHz and L2 \sim 1.2 GHz) transmitted by four GNSS constellations: GPS, Globalnaya Navigatsionnya Sputnikovaya Sistema (GLONASS), Galileo and Beidou.

The high sampling rate (20 Hz) of the commercial off-the-shelf GNSS receiver used by ScintPi 3.0 allows a direct estimate of the amplitude scintillation index (S₄) which can be described as the standard deviation of the signal intensity (*I*) normalized by its mean. S₄ indices are computed using 1 minute of measurements, that is, 1200 samples (Beach and Kintner, 2001):

$$S_4 = \sqrt{\frac{\langle I^2 \rangle - \langle I \rangle^2}{\langle I \rangle^2}}.$$
 (1)

The angle brackets in Equation 1 represent ensemble averaging but, in practice, time averages were used.

In addition to using Signal-to-Noise Ratio (SNR) values to estimate S₄, the pseudo-ranges and carrier phases were used to estimate the ionospheric TEC along the propagation path between receivers and satellites (e.g., Ciraolo et al., 2007; Oliveira et al., 2020). The receiver antennas were carefully deployed to minimize as much as possible multipath effects. Nevertheless, as an additional precaution, we only used data from satellites with elevation angles greater than 10° in this study.

Figure 1 presents one example of the measurements produced by the ScintPi 3.0 monitors deployed in Puerto Rico. In this example, the three monitors in Puerto Rico detected a severe scintillation event on the L-band signals transmitted by the GPS SVID 14 (SVID stands for Space-Vehicle Identification).

Figure 1 (a) shows the SNR values for the L1 signal measured by the ScintPi 3.0 monitors in Arecibo (red), Quebradillas (blue), and Culebra (green). For better visualization, the time series of the SNR for Quebradillas, Arecibo, and Culebra are presented shifted by +10 dB, -10 dB,

and ± 20 dB, respectively. Amplitude fading reaching 20 dB or more can be seen in the measurements. Figure 1 (b) shows the S₄ values estimated from the L1 SNR measurements. The S₄ values reveal the occurrence of intense scintillation (S₄ \geq 1) in the signals tracked by all the monitors. Finally, Figure 1 (c) shows relative ionospheric slant TEC measurements estimated from the phase measurements of the L1 and L2 signals transmitted by GPS SVID 14. The TEC measurements reveal the occurrence of long duration (10s of minutes) deep (several TEC units - TECu) ionospheric plasma depletions that are concurrent to the development of intense scintillation. The high-rate TEC measurements also allow the detection of short duration (< 1 minute) TEC fluctuations associated with small-scale ionospheric irregularities that accompany the large-scale plasma depletions.

Geomagnetic activity is known to affect the development of ionospheric irregularities and the occurrence of scintillation (e.g., Aarons, 1991; Basu et al., 2002; Ledvina et al., 2002). The thermospheric and ionospheric behavior and the relative contribution of different processes associated with plasma instabilities (e.g., prompt penetration electric fields, disturbed thermospheric winds, disturbed-dynamo electric fields, traveling ionospheric disturbances, etc.) vary from storm to storm. This is what has led scintillation events associated with geomagnetic storms to be studied and reported in a case-by-case basis. The analyses of storm-related events detected by the monitors in PR will be investigated in the future and is outside the scope of this study. As previously mentioned in section 2, only geomagnetic quiet nights were analyzed.

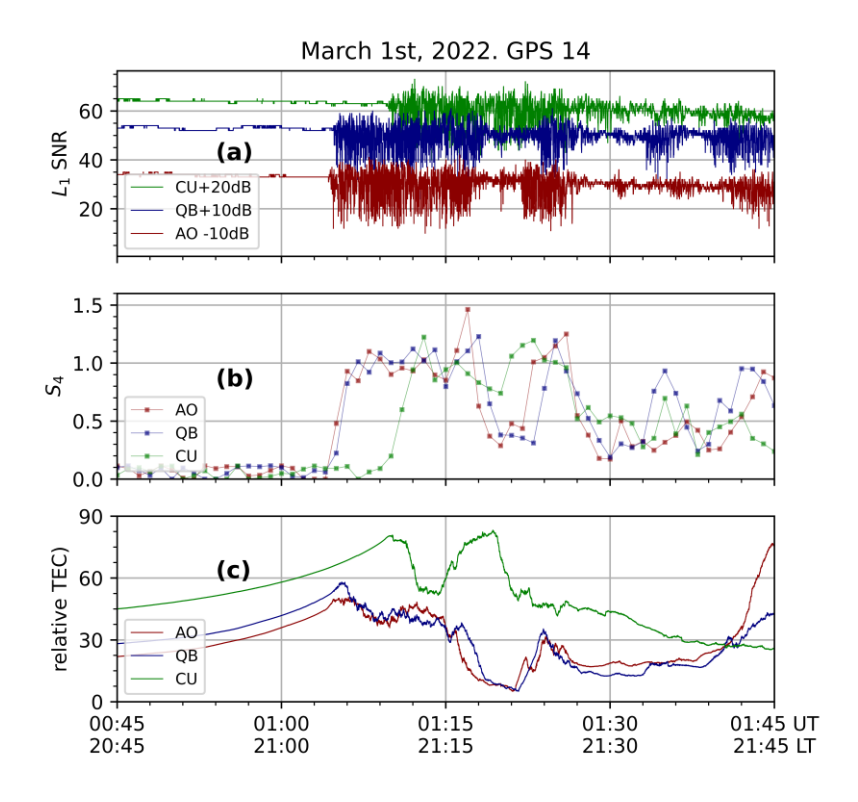


Figure 1 – Example of measurements made by the ScintPi 3.0 monitors in Puerto Rico. Panel (a): SNR for the L1 signal transmitted by GPS SVID 14 and received by the three monitors in PR on March 1, 2022. Panel (b): S₄ index computed for the L1 signals shown in panel (a). Panel (c): Relative TEC estimated from GPS SVID 14 L1 and L2 signals. LT refers to Atlantic Standard Time (AST).

2.2 GOLD measurements

The Global-scale Observations of the Limb and Disk (GOLD) mission, hosted by the geostationary satellite SES-14 in orbit at 47.5°W, has a dual-channel ultraviolet imaging spectrograph producing global-scale, high-cadence images, covering both hemispheres over the Atlantic and American region (Eastes et al., 2017). This mission was launched on January 25th, 2018 and is providing high-level data since October 5th, 2018.

In support of our ground-based observations we used the nighttime scans level 2 data labeled NMAX. The NMAX is a georeferenced quantity that corresponds to the peak electron density in the F-region and can be used to build maps of the ionospheric F-region morphology over the region of interest (Caribbean sector) from 23:20 UT to 00:40 UT of the next day. These maps can provide important information about the ionospheric conditions leading to the scintillation and TEC profiles recorded by the ground-based monitors.

3. Results and Discussion

In this section we present and discuss results related to the severity, occurrence rate, spatiotemporal distribution, and the source of the scintillation events during geomagnetically quiet conditions.

3.1 On the severity and occurrence rate of quiet-time scintillation events

Figure 2 shows examples of measurements of ionospheric scintillation made by the Arecibo monitor over four consecutive days. It shows the S₄ values of L1 (gray) and L2 (red) signals for all the satellites above 10° elevation tracked by the monitor. The values of the 3-hour Kp index are also presented (blue line).

On February 17^{th} , 2022, the S_4 values remained at background levels, but on February 18^{th} , 19^{th} , and 20^{th} , the monitor recorded $S_4 > 1$ for L1 and L2 during nighttime (20:00-00:00 LT). We point out that most of the period was under geomagnetically quiet conditions except for February 20^{th} , 2022, starting at around 00:00 UT. An additional magenta dashed line was used to facilitate the identification of occurrences of Kp index above the threshold for the geomagnetically quiet condition (Kp = 3).

Figure 2 serves to show that ionospheric scintillation can be observed on signals measured by a receiver located in PR even under geomagnetically quiet conditions. Furthermore, it shows that scintillation events can be severe with S₄ values exceeding 1 for both L1 and L2 at times.

Next, Figure 3 shows a summary of the scintillation observations over the 3-month period of interest, here made by the Arecibo monitor. It displays the S_4 values for all satellites with elevation greater than 10° for the period between 23:00 and 11:00 UT ($\sim 19:00$ and $\sim 07:00$ LT). Only data from geomagnetically quiet conditions are shown. A total of 43 quiet days were identified in the 90-day campaign period used in this study.

The first noteworthy feature that can be observed in the measurements presented in Figure 3 is the common occurrence of intense scintillation. The measurements show that, even under geomagnetically quiet conditions, scintillation can be observed in most days. To better quantify

the scintillation occurrence rate, we first defined a scintillation detection threshold. We considered that scintillation was observed on a given night if $S_4 \ge 0.3$ on the L1 signal occurred in at least 10 measurements between 23:00 and 11:00 UT. The nights when scintillation was not identified are indicated by the green date panels in Figure 3. With that definition, we found that scintillation was observed on 34 of the 43 geomagnetically quiet nights, that is, an occurrence rate of ~80%. Additionally, the results in Figure 3 show that intense scintillation, with S_4 often reaching and exceeding 1.0, are commonly observed by a GNSS receiver located in PR. Intense scintillation is observed in both frequencies, L1 and L2. Inspection of the data shows that the L2 signals suffer more intense scintillation than L1 signals. This is not a new finding and it is expected from previous theoretical and experimental studies (e.g., Yeh and Liu, 1982). Scintillation is frequency dependent with lower frequency signals being more affected compared to higher frequency signals.

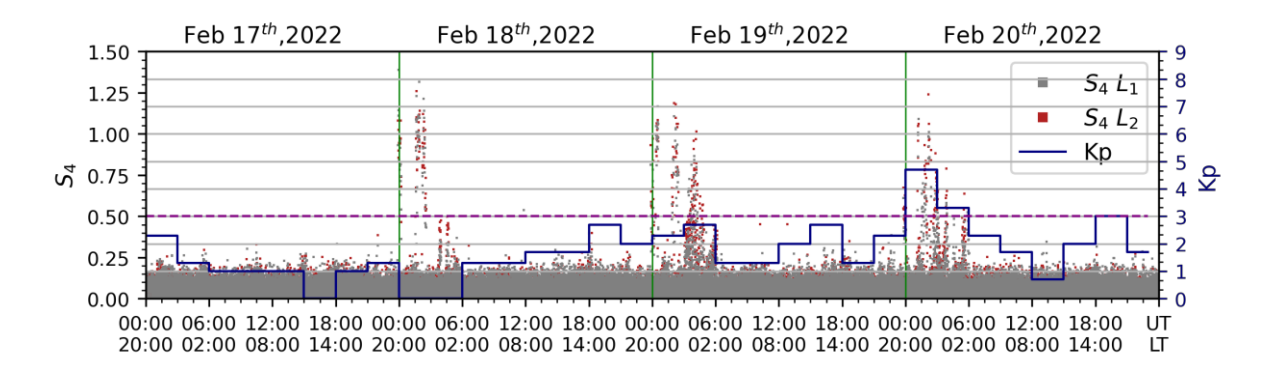


Figure 2 – Example of Arecibo S_4 measurements made between Feb 17^{th} to 20^{th} 2022. Gray and red markers correspond to S_4 measurements from L1 (~1.6 GHz) and L2 (~1.2 GHz) bands, respectively. Solid blue line indicates the Kp index, and the dashed purple line is the threshold taken into account to consider geomagnetically quiet time, both are related to the right-hand vertical axis. The horizontal axis represents the universal and local times over the days indicated above each panel. The vertical green lines separate the data in days. The example illustrates the occurrence of intense scintillation during geomagnetically quiet conditions (Feb. 18^{th} and 19^{th}). February 20^{th} is shown to illustrate a case when the Kp indices do not meet the requirements for a geomagnetically quiet day. LT refers to Atlantic Standard Time (AST).

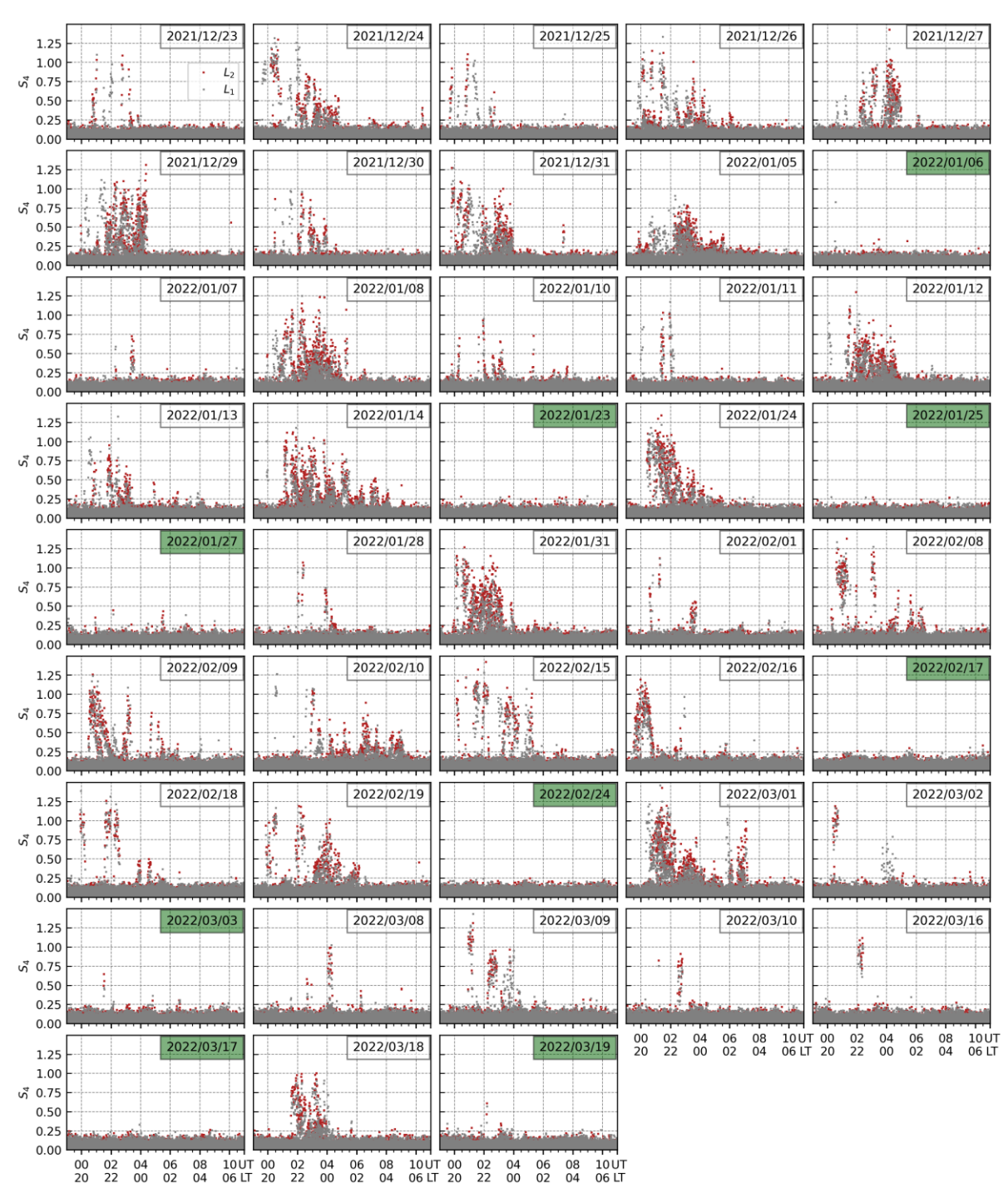


Figure 3 – Summary of scintillation activity observed by the Arecibo ScintPi 3.0 monitor. All the geomagnetically quiet nights between December 21^{st} , 2021, and March 20^{th} , 2022, are shown. The panels with date highlighted in green correspond to nights when no significant scintillation activity was identified, that is, when $S_4 \geq 0.3$ was observed in less than 10 measurements. LT refers to Atlantic Standard Time (AST).

3.2 On the spatio-temporal distribution of quiet-time scintillation events

We were also interested in the spatio-temporal distribution of the geomagnetically quiet-time scintillation activity observed by the monitors in PR as it can provide insights on the source of the ionospheric irregularities producing scintillation. For this analysis, we determined the

Ionospheric Pierce Points (IPPs) of the GNSS signals. The IPPs were calculated assuming the nominal altitude of the ionospheric F-region peak, that is, 350 km.

Next, we defined spatial bins of $2.5^{\circ} \times 2.5^{\circ}$ (geographic latitude \times geographic longitude) and considered time intervals of 1 hour. For each 1-hour interval considered, the occurrence rate was computed using the ratio of cases of $S_4(L1) \ge 0.3$ over the total number of observations within each bin for all the 43 geomagnetically quiet nights. Data from the three receivers were used and the occurrence rate was computed only for bins with at least 20 observations of $S_4(L1) \ge 0.3$.

Figure 4 summarizes the distribution of observed scintillation as a function of latitude and longitude for different 1-hour segments. It shows maps of the occurrence rate (colors) of scintillation $[S_4(L1) \ge 0.3]$ using the quiet observations made by the three scintillation monitors (red triangles). For reference, circles of elevation angles (green dashed lines) with respect to the position of the monitors and the location of dip latitudes (blue solid lines) are also shown. The dip latitudes were calculated using the International Geomagnetic Reference Field (IGRF-13) (Alken et al., 2021). The gray-shaded bins correspond to regions where the number of observations is less than 200 or outside the field of view for the entire quiet period within the campaign.

The results in Figure 4 show that the spatio-temporal evolution of the quiet-time scintillation events is limited to the southeast (magnetic south) of Puerto Rico. The events are first observed at lower geomagnetic latitudes and extend to higher latitudes as time progresses. The highest occurrence rates are seen between 00:00 UT and 04:00 UT (~20:00 and ~00:00 LT). The results also show that, for the set of observations analyzed here, the detection of significant scintillation is limited mostly to regions below 22° N dip latitude. However, a few cases can be seen reaching latitudes closer to Puerto Rico. See for instance, results for 02:00-03:00 UT in Figure 4.

3.3 On the source of quiet-time scintillation events

The results presented in Figure 4 indicate that the source of the ionospheric scintillation observed by the receivers in Puerto Rico is likely to originate at low latitudes, propagating to higher latitudes as time progresses. This observation suggests that the scintillation events could be associated with equatorial plasma bubbles. Additionally, it indicates that at least some of the quiet-time EPBs must be reaching as far as 22° N magnetic dip latitude (~ 1430 km magnetic apex heights).

Measurements such as those presented in Figure 1(c) also show that intense scintillation events were accompanied by large TEC depletions, which is also a feature of EPB-driven scintillations (Kintner et al., 2007). The timing of the occurrence rates also indicates that the observed scintillation events are associated with EPBs. Finally, the three-month observation campaign covers December to March, well within the ESF season in the American sector (e.g., Sobral et al., 2002).

To confirm that EPBs are the source of the scintillation events observed by the monitors in PR we analyzed the NMAX data provided by the GOLD mission over the American sector. GOLD NMAX data for the longitude sector of interest are available between ~23:20-00:40 UT (~19:20 and 20:40 LT).

Figure 5 shows georeferenced NMAX data from days previously exhibited in Figure 2. The bands of enhanced NMAX (yellow bands) nearly parallel to the magnetic equator are the Equatorial Ionization Anomaly (EIA) peaks. The blue streaks nearly perpendicular to the magnetic equator are NMAX depletions caused by EPBs. For reference, the red dashed circles indicate the elevation angles with respect to the location of the Arecibo monitor. The red solid lines indicate the magnetic dip latitudes. We remind the reader that Feb. 17th, 18th, and 19th were geomagnetically quiet days while Feb. 20th was considered geomagnetically disturbed.

Figure 5 serves to confirm that EPBs can reach the field of view of the receivers located in PR and be the source of the observed scintillations. For instance, Feb. 18th shows an EPB reaching about 18° N dip latitude and close to ~20° elevation angle of the Arecibo monitor. Severe scintillation was observed by the Arecibo monitor on that night and around that time. On the other hand, no scintillation was observed on Feb. 17th when a poorly developed EPB that only reached about 10° N dip latitude and did not enter the field of view of the Arecibo monitor. As a result, no scintillations were observed on that night.

EPBs are plasma structures aligned with the geomagnetic field and, therefore, they are expected to enter the field of view of the PR monitors from the southeastern direction propagating poleward. This is the same pattern of the scintillation occurrence rate revealed in Figure 4.

GOLD observations also show that the EIA northern crest reaches the field of view of the PR monitors even during geomagnetically quiet periods. In the examples presented in Figure 5, the northern EIA crest reaches the southeast field of view of the monitors, coinciding with the region of higher scintillation occurrence rate shown in Figure 4. The severity of amplitude scintillation as measured by the S₄ is known to increase in regions of enhanced background plasma density (e.g., Basu et al., 1988; Beach and Kintner, 2001). Therefore, GOLD images confirm background plasma conditions favoring the occurrence of intense scintillation on the GNSS signals.

Finally, the GOLD observations in Figure 5 also serve to show that the day-to-day variability in scintillation occurrence observed by the monitors in PR (see Figure 3) is not only controlled by the day-to-day variability in ESF occurrence but also by the day-to-day variability in the vertical development of EPBs. Mendillo et al. (2005) argued that EPBs would stop rising when the flux-tube integrated electron density inside the EPB matched the flux-tube integrated density of the surrounding background ionospheric plasma. Krall et al. (2010) confirmed this proposition using numerical simulations. Therefore, the variability of the vertical (or latitudinal) extent of EPBs would be controlled by the variability in the flux-tube integrated ionospheric plasma densities.

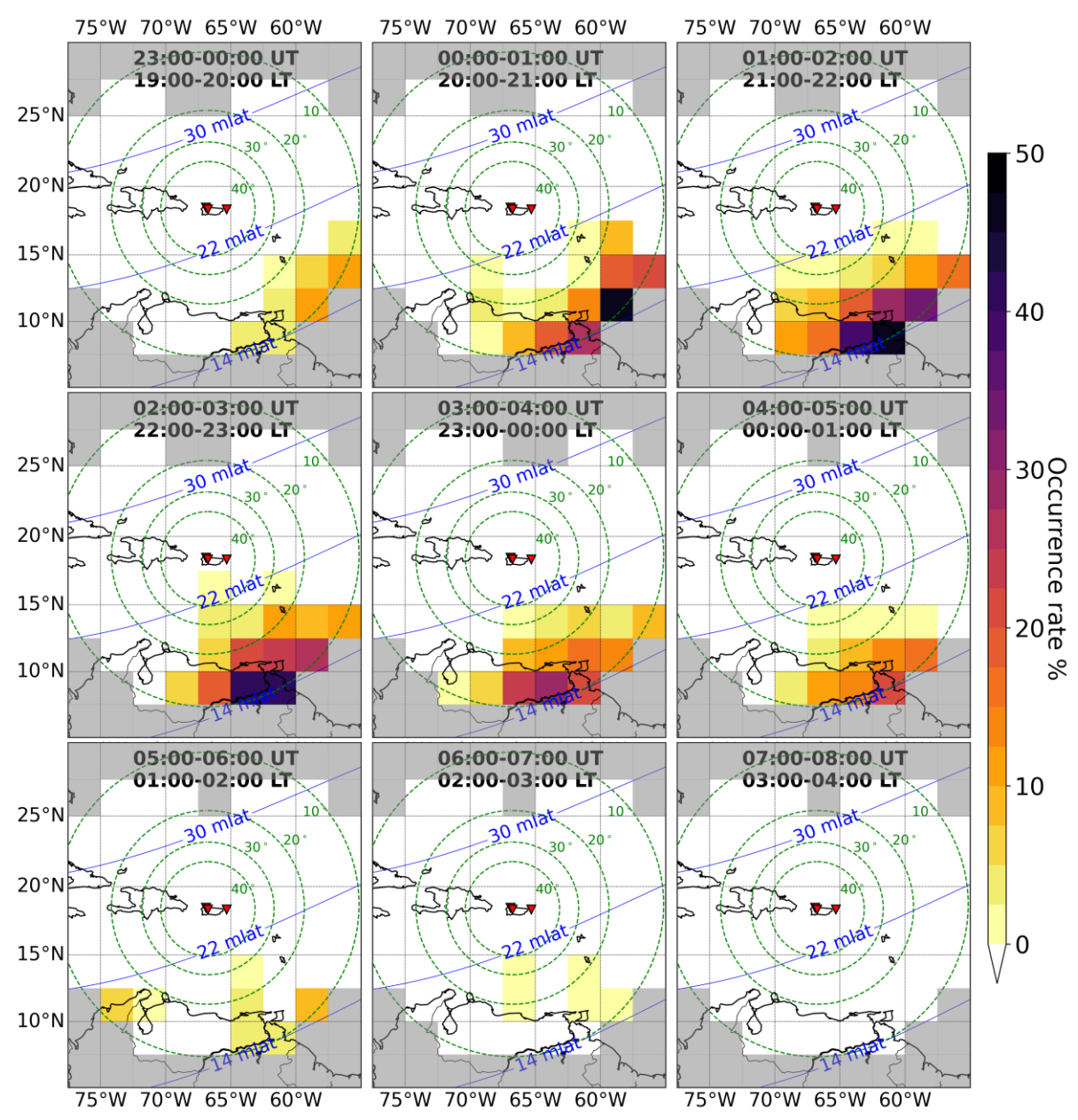


Figure 4 – Sequence of maps showing the spatio-temporal evolution of quiet-time L-band scintillations as observed by the three ScintPi 3.0 monitors deployed in Puerto Rico (red triangles) for the campaign period (December 21st, 2021 – March 20th, 2022). The occurrence rate is represented by the colors related to the color bar at the right. The gray-shaded bins correspond to regions where the number of observations is less than 200 or outside the field of view. The green dashed circles locate the IPPs (at 350 km) for different elevation angles with respect to the Arecibo station. The blue solid lines indicate dip latitudes isolines. LT refers to Atlantic Standard Time (AST).

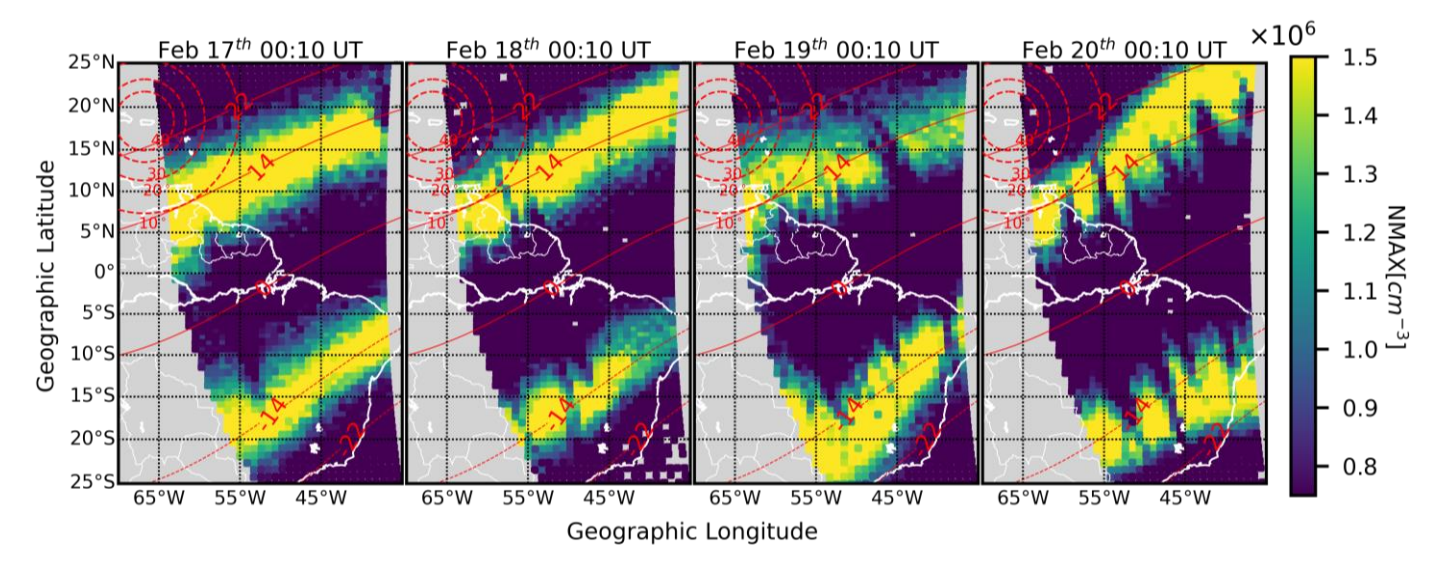


Figure 5 – Maps of F-region peak density (NMAX) provided by the GOLD mission for 00:10 UT and for the three quiet and one disturbed night (Feb. 20th) shown in Figure 2. The red dashed circles indicate the IPPs (at 350 km) for different elevation angles with respect to the Arecibo station. The red solid lines indicate dip latitudes. The GOLD images confirm that scintillation is observed when equatorial plasma bubbles reach the field of view of the PR receivers.

4. Conclusions

An increasing number of studies have been reporting the occurrence of ionospheric irregularities at mid-latitudes (Cherniak and Zakharenkova, 2016, 2022; Katamzi-Joseph et al., 2017; Aa et al., 2018; Li et al., 2018; Zakharenkova and Cherniak, 2020, 2021; and Sori et al., 2022). The majority of these studies, however, described case studies observed during geomagnetically disturbed conditions. Additionally, at times, the source of these plasma irregularities is difficult to determine unambiguously (Martinis et al., 2015; Kil et al., 2016).

In December 2021 three GNSS-based ionospheric scintillation and TEC monitors were installed in Puerto Rico (~24.5° N dip latitude) as part of an experimental effort to better understand mid-latitude irregularities and scintillation. The deployment and the study here targeted, more specifically, a better understanding of the coupling of low to mid latitudes during geomagnetically quiet conditions.

We report results of a comprehensive analysis of the first three months of observations (from December 21st, 2021, to March 20th, 2022). Observations made during geomagnetically quiet times were identified and the analyses focused on the occurrence rate, severity, spatio-temporal distribution, and origin of the scintillation events detected. Our interpretation of the ground-based observations was assisted by spaced-based measurements provided by the GOLD mission.

The main findings can be summarized as follows:

• Over a period of 90 consecutive nights (Dec. 21st, 2021 – Mar. 20th, 2022), 43 nights were under geomagnetically quiet conditions. The occurrence rate of L-band scintillation within these nights was ~80%, that is, scintillation was observed in 34 of the 43 nights. Perhaps

- more importantly, severe scintillation events ($S_4 \ge 1.0$) were observed in most cases. Finally, the scintillation events were accompanied by deep ionospheric TEC depletions.
- The spatio-temporal distribution of the scintillation events indicate that scintillation-producing irregularities occurred, predominantly, to the southeast of PR. This occurrence suggests that the source of the plasma irregularities is located at low dip latitudes. Also, 22° N dip latitude seems to be the upper boundary, at least for the quiet-time scintillation events detected in this campaign over the Caribbean region. The study stablishes a baseline for studies of the latitudinal reach of EPBs and scintillation. Future studies will investigate the response of the latitudinal reach for different geomagnetic conditions and variations in solar flux activity, for instance.
- Simultaneous space-based observations of the F-region peak electron densities made by the GOLD mission confirmed, conclusively, that EPBs were the source of irregularities causing scintillation. Even during geomagnetically quiet times, EPBs commonly reach the field of view of the PR monitors, that is, dip latitudes greater than 14° N. The observations also show that quiet-time scintillation is sometimes observed at dip latitudes as high as 18° N. Additionally, GOLD shows that the EIA and EPBs are more likely to reach the southeast region of PR which explains the spatio-temporal behaviour of scintillation and occurrence rates of scintillation in that area (Figure 4).
- Furthermore, GOLD shows the development of the northern crest of the EIA reaching the field of view of the PR monitors. Therefore, GOLD confirms the occurrence of the enhanced background plasma conditions required for the observed severe scintillation events.

5. Acknowledgements

Work at UT Dallas was supported by NSF Awards AGS- 2122639 and AGS-1916055. Differential code biases (DCBs) were obtained through the online archives of the Crustal Dynamics Data Information System (CDDIS), NASA Goddard Space Flight Center, Greenbelt, MD, USA. The Arecibo Observatory is operated by the University of Central Florida under a cooperative agreement with the National Science Foundation (AST-1744119) and in alliance with Yang Enterprises and Ana G. Méndez-Universidad Metropolitana. CGMB and PT would like to thank the support from NSF Award AGS-2221770. GOLD is supported by NASA contract 80GSFC18C0061 to the University of Colorado. The authors thank Mr. Carlos Pérez for hosting the ScintiPi 3.0 deployed at Quebradillas.

6. Availability of data and materials

The **GOLD** data is available **GOLD** Science Data Center at (https://gold.cs.ucf.edu/data/search/) and at NASA's **Physics** Data Facility Space (http://spdf.gsfc.nasa.gov/). Geomagnetic indices may be accessed https://omniweb.gsfc.nasa.gov/form/omni min.html. Ionospheric scintillation and TEC data used in this study will be made available through public repository (zenodo.org) prior to publication if accepted.

IGRF-13 can be accessed at https://www.ngdc.noaa.gov/IAGA/vmod/igrf.html

References

Aa, E.; Huang, W.; Liu, S.; Ridley, A.; Zou, S.; Shi, L.; Chen, Y.; Shen, H.; Yuan, T.; Li, J.; and T. Wang (2018). Midlatitude Plasma Bubbles Over China and Adjacent Areas During a Magnetic Storm on 8 September 2017. Space Weather, v. 16 (3), p. 321-331, doi: 10.1002/2017SW001776.

Aarons, J. (1982). Global morphology of ionospheric scintillations. Proceedings of the IEEE, v. 70 (4), p. 360-378, doi: 10.1109/PROC.1982.12314.

Aarons J (1991). The role of the ring current in the generation or inhibition of equatorial F-layer irregularities during magnetic storms. Radio Sci 26:1131–1149

Afraimovich, E. L.; Astafyeva, E. I.; Berngardt, O. I.; Demyanov, T. N.; Kondakova, B. G.; Lesyuta, O. S.; and B. G. Shpynev (2004). Mid-latitude amplitude scintillations of GPS signals and GPS failures at the auroral oval boundary. Radiophysics and Quantum Electronics, v. 47 (7), p. 453-468, doi: 10.1023/B:RAQE.0000047237.67771.bc.

Afraimovich, E. L.; Astafyeva, E. I.; Demyanov, V. V.; and I. F. Gamayunov (2009). Midlatitude amplitude scintillation of GPS signals and GPS performance slips. Advances in Space Research, v. 43 (6), p. 964-972, doi: 10.1016/j.asr.2008.09.015.

Alken P, Thébault E, Beggan CD, Amit H, Aubert J, Baerenzung J, Bondar TN, Brown WJ, Califf S, Chambodut A, Chulliat A, Cox GA, Finlay CC, Fournier A, Gillet N, Grayver A, Hammer MD, Holschneider M, Huder L, Hulot G, Jager T, Kloss C, Korte M, Kuang W, Kuvshinov A, Langlais B, Léger JM, Lesur V, Livermore PW, Lowes FJ, Macmillan S, Magnes W, Mandea M, Marsal S, Matzka J, Metman MC, Minami T, Morschhauser A, Mound JE, Nair M, Nakano S, Olsen N, Pavón-Carrasco FJ, Petrov VG, Ropp G, Rother M, Sabaka TJ, Sanchez S, Saturnino D, Schnepf NR, Shen X, Stolle C, Tangborn A, Tøffner-Clausen L, Toh H, Torta JM, Varner J, Vervelidou F, Vigneron P, Wardinski I, Wicht J, Woods A, Yang Y, Zeren Z, Zhou B (2021) International Geomagnetic Reference Field: the thirteenth generation. Earth, Planets and Space 73(49):1-25. https://doi.org/10.1186/s40623-020-01288-x

Basu, S.; MacKenzie, E.; and S. Basu (1988). Ionospheric constraints on VHF/UHF communications links during solar maximum and minimum periods. Radio Science, v. 23 (3), p. 363–378, doi:10.1029/RS023i003p00363.

Basu, S.; Basu, S.; Valladares, C. E.; Yeh, H. C.; MacKenzie, E.; Sultan, P. J.; Aarons, J.; Rich, F. J.; Doherty, P.; Groves, K. M.; and T. W. Bullett (2001). Ionospheric effects of major magnetic storms during the International Space Weather period of September and October 1999: GPS observations, VHF/UHF scintillations, and in situ density structures at middle and equatorial latitudes. Journal of Geophysical Research: Space Physics, v. 106 (A12), p. 30389-30413, doi: 10.1029/2001JA001116.

Basu, S., Groves, K.M., Basu, Su. and P.J. Sultan (2002). Specification and forecasting of scintillations in communication/navigation links: current status and future plans. Journal of Atmospheric and Solar-Terrestrial Physics, Volume 64, Issue 16, Pages 1745-1754, ISSN 1364-6826, https://doi.org/10.1016/S1364-6826(02)00124-4.

Beach, T.; and P. M. Kintner (2001). Development and use of a GPS ionospheric scintillation monitor. IEEE Transactions on Geoscience and Remote Sensing, v. 39 (5), p. 918-928, doi: 10.1109/36.921409.

Blanc, M.; A. D. Richmond (1980). The ionospheric disturbance dynamo. Journal of Geophysical Research: Space Physics, v. 85 (A4), p. 1669-1686, doi: 10.1029/JA085iA04p01669.

Briggs, B. H. (1964). Observations of radio star scintillations and spread-F echoes over a solar cycle. Journal of Atmospheric and Terrestrial Physics, v. 26 (1), p. 1-23, doi: 10.1016/0021-9169(64)90104-7.

Cherniak, I.; and I. Zakharenkova (2016). First observations of super plasma bubbles in Europe. Geophysical Research Letters, v. 43 (21), p. 11137-11145, doi: 10.1002/2016GL071421.

Cherniak, I.; and I. Zakharenkova (2022). Development of the storm-induced ionospheric irregularities at equatorial and middle latitudes during the 25-26 August 2018 geomagnetic storm. Space Weather, v. 20 (2), p. 1-18, doi: 10.1029/2021SW002891.

Ciraolo, L.; Brunini, C.; Meza, A.; and S. M. Radicella (2007). Calibration errors on experimental slant total electron content (TEC) determined with GPS. Journal of Geodesy, v. 81, p. 111-120, doi: 10.1007/s00190-006-0093-1.

Eastes, R. W.; McClintock, W. E.; Burns, A. G.; Anderson, D. N.; Anderson, L.; Codrescu, M.; Correira, J. T.; Daniell, R. E.; England, S. L.; Evans, J. S.; Harvey, L.; Krywonos, A.; Lumpe, J. D.; Richmond, A. D.; Rusch, D. W.; Siegmund, O.; Solomon, S. C.; Strickland, D. J.; Woods, T. N.; Aksnes, A.; Budzien, S. A.; Dymond, K. F.; Eparvier, F. G.; Martinis, C. R.; and J. Oberheide (2017). The Global-Scale Observations of the Limb and Disk (GOLD) mission. Space Science Reviews, v. 212, p. 383-408, doi: 10.1007/s11214-017-0392-2.

Fukao, S.; Kelley, M. C.; Shirakawa, T.; Takami, T.; Yamamoto, M.; Tsuda, T.; and S. Kato (1991). Turbulent upwelling of the mid-latitude ionosphere: 1. Observational results by the MU radar. Journal of Geophysical Research: Space Physics, v. 96 (A3), p. 3725-3746, doi: 10.1029/90JA02253.

Gomez Socola, J., Rodrigues, F.S. (2022). ScintPi 2.0 and 3.0: low-cost GNSS-based monitors of ionospheric scintillation and total electron content. Earth Planets Space 74, 185. https://doi.org/10.1186/s40623-022-01743-x.

Hysell, D. L. (2000), An overview and synthesis of plasma irregularities in equatorial spread F, Journal of Atmospheric and Solar-Terrestrial Physics, 62, 12, 2000, 1037-1056, 1364-6826, https://doi.org/10.1016/S1364-6826(00)00095-X.

Hysell, D.; Larsen, M.; Fritts, D.; Laughman, B.; and M. Sulzer (2018). Major upwelling and overturning in the mid-latitude F region ionosphere. Nature Communications, v. 9 (3326), p. 1-11, doi: 10.1038/s41467-018-05809-x.

Jakowski, N.; Mayer, C.; Wilken, V.; and C. Borries (2007). Ionospheric storms at high and mid-latitudes monitored by ground and space based GPS techniques. Proceedings of the

- International Beacon Satellite Symposium, June 11-15, 2007, edited by P. H. Doherty, Boston College, Chestnut Hill, Massachussets.
- Jiao, Y.; and Y. T. Morton (2015). Comparison of the effect of high-latitude and equatoria ionospheric scintillation on GPS signals during the maximum of solar cycle 24. Radio Science, v. 50 (9), p. 886-903, doi: 10.1002/2015RS005719.
- Juan, J. M.; Sanz, J.; González-Casado, G.; Rovira-Garcia, A.; Camps, A.; Riba, J.; Barbosa, J.; Blanch, E.; Altadill, D.; and R. O. Perez (2018). Feasibility of precise navigation in high and low latitude regions under scintillation conditions. Journal of Space Weather and Space Climate, v. 8 (A05), p. 1-11, doi: 10.1051/swsc/2017047.
- Karasawa, Y.; Yasukawa, K.; and M. Yamada (1985). Ionospheric scintillation measurements at 1.5 GHz in mid-latitude region. Radio Science, v. 20 (3), p. 643-651, doi: 10.1029/RS020i003p00643.
- Katamzi-Joseph, Z. T.; Habarulema, J. B.; and M. Hernández-Pajares (2017). Midlatitude postsunset plasma bubbles observed over Europe during intense storms in April 2000 and 2001. Space Weather, v. 15 (9), p. 1177-1190, doi: 10.1002/2017SW001674.
- Kelley, M. C.; and S. Fukao (1991). Turbulent upwelling of the mid-latitude ionosphere: 2. Theoretical framework. Journal of Geophysical Research: Space Physics, v. 96 (A3), p. 3747-3753, doi: 10.1029/90JA02252.
- Kelley, M. C.; Makela, J. J.; Swartz, W. E.; Collins, S. C.; Thonnard, S.; Aponte, N.; and C. A. Tepley (2000a). Caribbean Ionosphere Campaign, year one: Airglow and plasma observations during two intense mid-latitude spread-*F* events. Geophysical Research Letters, v. 27 (18), p. 2825-2828, doi: 10.1029/2000GL000022.
- Kelley, M. C.; Garcia, F.; Makela, J. J.; Fan, T.; Mak, E.; Sia, C.; and D. Alcocer (2000b). Highly structured tropical airglow and TEC signatures during strong geomagnetic activity. Geophysical Research Letters, v. 27 (4), p. 465-468, doi: 10.1029/1999GL900598.
- Kelley, M. C.; Swartz, W. E.; and J. J. Makela (2004). Mid-latitude ionospheric fluctuation spectra due to secondary instabilities. Journal of Atmospheric and Solar-Terrestrial Physics, v. 66 (17), p. 1559-1565, doi: 10.1016/j.jastp.2004.07.004.
- Kil, H.; Miller, E. S.; Jee, G.; Kwak, Y. S.; Zhang, Y.; and M. Nishioka (2016). Comment on "The night when the auroral and equatorial ionospheres converged" by Martinis, C., J., Baumgardner, M. Mendillo, J. Wroten, A. Coster, and L. Paxton. Journal of Geophysical Research: Space Physics, v. 121 (10), p. 10599-10607, doi: 10.1002/2016JA022662.
- Kintner, P. M.; Ledvina, B. M.; and E. R. de Paula (2007). GPS and ionospheric scintillations. Space Weather, v. 5 (9), p. 1-23, doi: 10.1029/2006SW000260.
- Ledvina, B. M.; Makela, J. J.; and P. M. Kintner (2002). First observations of intense GPS L1 amplitude scintillations at midlatitude. Geophysical Research Letters, v. 29 (14), p. 1-4, doi: 10.1029/2002GL014770.

- Li, G.; Ning, B.; Wang, C.; Abdu, M. A; Otsuka, Y.; Yamamoto, M.; Wu, J.; and J. Chen (2018). Storm-enhanced development of postsunset equatorial plasma bubbles around the meridian 120°E/60°W on 7-8 September 2017. Journal of Geophysical Research: Space Physics, v. 123 (9), p. 7985-7998, doi: 10.1029/2018JA025871.
- Krall J, Huba JD, Ossakow SL, Joyce G (2010) Why do equatorial ionospheric bubbles stop rise? Geophys Res Lett 37(L09105):1–4. https://doi.org/10.1029/2010GL043128
- Martinis, C.; and M. Mendillo (2007). Equatorial spread F-related airglow depletions at Arecibo and conjugate observations. Journal of Geophysical Research: Space Physics, v. 112 (A12), p. 1-9, doi: 10.1029/2007JA012403.
- Martinis, C.; Baumgardner, J.; Mendillo, M.; Su, S. Y.; and N. Aponte (2009). Brightening of 630.0 nm equatorial spread-F airglow depletions. Journal of Geophysical Research: Space Physics, v. 114 (A06318), p. 1-9, doi: 10.1029/2008JA013931.
- Martinis, C.; Baumgardner, J.; Mendillo, M.; Wroten, J.; Coster, A.; and L. J. Paxton (2015). The night when the auroral and equatorial ionospheres converged. Journal of Geophysical Research: Space Physics, v. 120 (9), p. 8085-8095, doi: 10.1002/2015JA021555.
- Mathews, J. D.; Machuga, D. W; and Q. Zhou (2001a). Evidence for electrodynamic linkages between spread-F, ion rain, the intermediate layer, and sporadic E: results from observations and simulations. Journal of Atmospheric and Solar-Terrestrial Physics, v. 63 (14), p. 1529-1543, doi: 10.1016/S1364-6826(01)00034-7.
- Mathews, J. D.; González, S.; Sulzer, M. P.; Zhou, Q. H.; Urbina, J.; Kudeki, E.; and S. Franke (2001b). Kilometer-scale layered structures inside spread-F. Geophysical Research Letters, v. 28 (22), p. 4167-4170, doi: 10.1029/2001GL013077.
- Mendillo, M.; Baumgardner, J.; Nottingham, D.; Aarons, J.; Reinisch, B. W.; Scali, J.; and M. C. Kelley (1997). Investigations of thermospheric-ionospheric dynamics with 6300-Å images from the Arecibo observatory. Journal of Geophysical Research: Space Physics, v. 102 (A4), p. 7331-7343, doi: 10.1029/96JA02786.
- Mendillo M, Zesta E, Shodhan S, Sultan PJ, Doe R, Sahai Y, Baumgardner J (2005) Observations and modeling of the coupled latitude-altitude patterns of equatorial plasma depletions. J Geophys Res Space Phys 110(A09303):1–7. https://doi.org/10.1029/2005JA011157
- Oliveira, C. B. A.; Espejo, T. M. S.; Moraes, A. O.; Costa, E.; Sousasantos, J.; Lourenço, L. F. D.; and M. A. Abdu (2020). Analysis of plasma bubble signatures in total electron content maps of the low-latitude ionosphere: A simplified methodology. Surveys in Geophysics, v. 41, p. 897-931, doi: 10.1007/s10712-020-09584-7.
- Perkins, F. (1973). Spread F and ionospheric currents. Journal of Geophysical Research, v. 78 (1), p. 218-226, doi: 10.1029/JA078i001p00218.
- Rodrigues, F. S.; Socola, J. G.; Moraes, A. O.; Martinis, C.; and D. A. Hickey (2021). On the properties of and ionospheric conditions associated with a mid-latitude scintillation event observed over southern United States. Space Weather, v. 19 (6), p. 1-20, doi: 10.1029/2021SW002744.

Senior, C.; and M. Blanc (1984). On the control of magnetospheric convection by spatial distribution of ionospheric conductivities. Journal of Geophysics Research: Space Physics, v. 89 (A1), p. 261-284, doi: 10.1029/JA089iA01p00261.

Sobral, J. H. A.; Abdu, M. A.; Takahashi, H.; Taylor, M. J.; de Paula, E. R.; Zamlutti, C. J.; de Aquino, M. G.; and G. L. Borba (2002). Ionospheric plasma bubble climatology over Brazil based on 22 years (1977-1998) of 630 nm airglow observations. Journal of Atmospheric and Solar-Terrestrial Physics, v. 64 (12-14), p. 1517-1524, doi: 10.1016/S1364-6826(02)00089-5. Sori, T.; Otsuka, Y.; Shinbori, A.; Nishioka, M.; and S. Perwitasari (2022). Geomagnetic conjugacy of plasma bubbles extending to mid-latitudes during a geomagnetic storm on March 1, 2013. Earth, Planets and Space, v. 74 (120), p. 1-16, doi: 10.1186/s40623-022-01682-7.

Sultan, P. J. (1996), Linear theory and modeling of the Rayleigh-Taylor instability leading to the occurrence of equatorial spread F, J. Geophys. Res., 101 (A12), 26875–26891, doi:10.1029/96JA00682.

Urbina, J.; Kudeki, E.; Franke, S. J.; Gonzalez, S.; Zhou, Q. and S. C. Collins (2000). 50 MHz radar observations f mid-latitude E-region irregularities at Camp Santiago, Puerto Rico. Geophysical Research Letters, v. 27 (18), p. 2853-2856, doi: 10.1029/2000GL000028.

Vadakke Veettil, S., Haralambous, H. & Aquino, M. (2017) Observations of quiet-time moderate midlatitude L-band scintillation in association with plasma bubbles. GPS Solut 21, 1113–1124. https://doi.org/10.1007/s10291-016-0598-x

Wolf, R. A. (1970). Effects of ionospheric conductivity on convective flow of plasma in the magnetosphere. Journal of geophysical Research, v. 75 (25), p. 4677-4698, doi: 10.1029/JA075i025p04677.

Yeh, K. C. and G. W. Swenson Jr. (1959). The scintillation of radio signals from satellites, J. Geophys.Res., 64, 2281-2286.

Yeh, K. C.; Liu, C. H. (1982). Radio wave scintillations in the ionosphere. Proceedings of the IEEE, v. 70 (4), p. 324-360, doi: 10.1109/PROC.1982.12313.

Zakharenkova, I.; and I. Cherniak (2020). When plasma streams tie up equatorial plasma irregularities with auroral ones. Space Weather, v. 18 (2), p. 1-19, doi: 10.1029/2019SW002375.

Zakharenkova, I.; and I. Cherniak (2021). Effects of storm-induced equatorial plasma bubbles on GPS-based kinematic positioning at equatorial and middle latitudes during the September 7–8, 2017, geomagnetic storm. GPS Solutions, v. 25 (132), p. 1-14, doi: 10.1007/s10291-021-01166-3.